Predicting Percolation Threshold value of EMI SE for Conducting Polymer Composite Systems through Different Sigmoidal Models

Mostafizur Rahaman[1]* □ Prashant Gupta[2] □ Mokarram Hossain[3] □ Ali Aldalbahi[1]*

[1]Department of Chemistry, College of Science, King Saud University, Riyadh, 11451, Saudi Arabia
[2]Department of Plastic and Polymer Engineering, Maharashtra Institute of Technology, Aurangabad 431010 Maharashtra
[3]Zienkiewicz Centre for Computational Engineering, College of Engineering, Swansea University, SA1 8EN, United Kingdom

***Corresponding author email id**: mrahaman@ksu.edu.sa (MR); aaldalbahi@ksu.edu.sa (AA)

Abstract

Like electrical conductivity, the electromagnetic interference shielding effectiveness (EMI SE) of carbon-containing polymeric composites also goes through a transition phase known as the percolation threshold (PT). In this study, the applicability of various sigmoidal models such as Sigmoidal–Boltzmann (SB), Sigmoidal–Dose Response (SD), Sigmoidal–Hill (SH), Sigmoidal–Logistic (SL), and Sigmoidal–Logistic-1 (SL-1) to determine the PT of EMI SE has been tested for composites of ethylene vinyl acetate (EVA) copolymer and acrylonitrile butadiene rubber (NBR) matrix reinforced with various particulate and fibrous carbon fillers. It is observed that the SB and SD models predicted similar PT. On the other hand, other models reported different values when validated for any particular composite system. The difference in results of PT has been discussed in detail from a viewpoint of the benefits and vice versa of these models. Also, the classical percolation theory has been applied to determine the PT of EMI SE for comparison with the values obtained through the sigmoidal models. In order to judge the universal acceptability of these models, the EMI SE results have been tested for various polymeric composites taken from some published literature. The results indicate that all the models except the SL-1 model can be successfully applied for predicting the PT of EMI SE for polymer composites.

Keywords Polymer composites □ EMI SE □ percolation threshold □ Sigmoidal models □ carbon filler

Introduction

The advancements in technology have a lot to offer in today's world. If we consider modern electronics, for instance, some of the everyday' use items without which the world becomes unimaginable today, these may include cell phones, computers, radio, microwaves, laptops, and associated smart devices. Even though a lot is on offer, the environmental hazard can't be neglected as these electronic devices emit electromagnetic radiation. Due to their ability to instigate health hazards, they can potentially be harmful to living beings. Some of the ill-effects include tissue damage, the formation of tumors, chances of infertility, etc.[1] Furthermore, they tend to cause electrical/electronic equipment to malfunction and disrupt the radio frequency spectrum, which are vital in defense, communication systems, appliances, and aerospace applications. They also have the potential to inflict huge damages around hazardous atmospheres by igniting flammable materials.[2] The growth of electronics in today's world is based on the versatility on offer for use in domestic households, commercial and industrial establishments in areas such as medical, automotive, aerospace, satellites, naval and air bases, etc. The emission of radiations in various frequency ranges from these electronic products creates an interference known as electromagnetic interference, which is capable of hampering the performance of such devices as a part of the system or whole.[1] To run smooth operation within the majority of these important agencies of national security, banking, etc., it is vital to have EMI shielding materials that are effective in blocking out these damaging radiations that may result in loss of life, money, etc.

Electromagnetic interference shielding effectiveness (EMI SE) is considered to be an amalgamation of surface reflection of the substrate related to the mismatch of impendence in between air and absorber with varying frequency, electromagnetic energy absorption or dissipation of energy due to interaction of absorber and radiation; and electromagnetic radiation-based reflections within the substrate material due to scattering observed as a result of heterogeneity in the substrate.[3,4] The materials capable to have EMI shielding properties are increasingly gaining its importance in various sectors such as aerospace,[5-7] communication, medicine,[8-10] commercial electronics[11-13] and defense applications[14-16] due to their effectiveness in shielding these harmful electromagnetic radiations. The suitable EMI shielding materials are obviously metals but their drawbacks such as tendency to oxidize and rust, high raw material cost, higher density and non-flexibility don't make them the automatic/right choice of material for use in such applications.[17,18] Polymers due to low cost, corrosion resistance, low weight, and ease in machining/manufacturing are more suitable

candidate compared to metals to be used for EMI shielding purposes.[19] As most of the polymers are insulators, the EMI shielding effect is not very prominent on their own, and hence there are the use of composites structure for imparting better EMI shielding in such cases.[20] Until now, many research work have been carried out to understand the mechanism of polymer composites for providing better EMI shielding.[21] Several composite systems such as graphene/epoxy,[22] single and multiwalled carbon nanotubes/epoxy,[23,24] graphene nanosheets/thermoplastic polyurethane,[25] etc. were prepared and studied their EMI SE characteristics. Cu based metal-polymer composites were reported in literatures where effective thermal dissipation was observed.[26,27] The EMI shielding effectiveness of polyaniline and different carbon-based composites was studied where the polyaniline was synthesized by chemical oxidative polymerization method.[28] The use of various fillers such as carbon black, graphene, carbon fiber, SWCNT, MWCNT, metal oxide fillers such as TiO_2, ceramic fillers, etc. have been reported for use in improvement of EMI shielding effectiveness characteristics. A number of standards such as ASTM D4935-99, ASTM ES7-83, IEEE-STD-299-1991, MIL-STD-188-125A, MIL-STD-462, and MIL-STD-461C can be employed to evaluate the effectiveness of EMI shielding. The most popular method is the coaxial transmission line method along with others such as the free space method, shielded room method, and shield box method.[29]

There is plenty of literature available on the study of EMI shielding effectiveness of polymer-based composites but none of the literature has discussed its percolation threshold (PT) phenomena. Like electrical conductivity, the value of PT for EMI SE can also be calculated using either classical percolation theory or Sigmoidal models. In our previous work, we have discussed about the determination of PT for electrical conductivity of polymer-based composites by both methodologies.[30] The intuition and theoretical background behind the proposition of these models that how these models can be used for the determination of percolation threshold are already mentioned therein. We mentioned about the origin of this concept and mathematically proved it. In another study, we have reported the PT values of EMI SE only by the use of SB model.[31] Thus, the objective of the present work is to determine the PT of EMI SE using different Sigmoidal models such as Boltzmann, Dose Response, Hill, Logistic, Logistic-1 as well as classical percolation theory and validate their suitability for polymer-based composites. These models have previously been proven effective for the determination of conductivity's PT but this attempt has been made for EMI SE, herein, for the first time.

Experimental

Materials

The polymeric matrix base materials, i.e., acrylonitrile butadiene rubber (NBR, with a Mooney viscosity, ML_{1+4} at 100 °C of 45) and ethylene vinyl acetate rubber (EVA-2806, with a Mooney viscosity, ML_{1+4} at 100 °C of 20) having vinyl acetate content of 28 % and melt flow index of 6 gm/10 min was provided by Japan Synthetic Rubber Co. Ltd and NOCIL, Mumbai, respectively. The fillers used in the composites i.e., conductex (SC Ultra bead) carbon black (CCB), printex XE2 carbon black (PCB), and short carbon fiber (SCF) were supplied by Columbian Chemicals Company-Atlanta, Degussa Canada Limited, and R K Carbon Fiber Leatherhead, UK. Dicumyl peroxide (DCP), which was used as a curing agent for the composite, with 98 % purity and a MP of 80 °C was procured from Aldrich Chemicals Company, USA. Tri Allyl Cyanurate (TAC), used as a co-vulcanizate, was supplied by E. Merck (India limited), India. 1, 2-Dihydro 2, 2, 4-trimethyl quinoline (TQ, polymerized) was supplied by Lanxess (India) Private Ltd.

Preparation of polymer composites

EVA and NBR based composites were prepared by compounding methodology using a Brabender Plasticorder (PLE 330, Brabender GmbH & Co. KG, Duisburg, Germany) and a two-roll mill (Santec Exim Pvt Ltd., Manesar, India). EVA and NBR were individually melted in Brabender at 120 °C for 6 min at 60 rpm for compaction of the polymer compound after melting. The carbon black fillers along with other formulation ingredients i.e., TQ, DCP and TAC were mixed with virgin EVA and NBR separately in the two-roll milling equipment at ambient temperature as per the sequence of the recipe given in Table I. Alternatively, SCFs were compounded in a Haake Rheocord under identical conditions i.e., 120 °C for 6 min at 60 rpm. The additives were taken on the basis of part per hundred parts of the polymer matrix. The volume ratio of polymer and additive were also determined as reported in Table I. The time for curing of various composites was quantified with a Monsanto rheometer R-100S (Gomaplast Machinery, Inc., Wooster, OH, USA) at 160 °C with a time duration of 1 h. The test specimens of various composites were made using a compression molding machine setup with a cure temperature of 160 °C for specified time of curing.

Table I Recipe for EVA and NBR composites

Ingredients	**Composition parts by phr (weight per hundred parts of polymer) and**

	V_f (Volume fraction of filler in polymer)			
	E_0N_{100} (phr)	E_0N_{100} (V_f)	$E_{100}N_0$ (phr)	$E_{100}N_0$ (V_f)
EVA	0	-	100	1
NBR	100	1	0	-
DCP	02	0.02	02	0.02
TAC	01	0.01	01	0.01
TQ	01	0.01	01	0.01
CCB	0, 10, 20, 30, 40, 50, 60	0, 0.051, 0.096, 0.139, 0.178, 0.213, 0.245	0, 10, 20, 30, 40, 50, 60	0, 0.051, 0.096, 0.139, 0.178, 0.213, 0.245
PCB	0, 10, 20, 30, 40, 50	0, 0.051, 0.096, 0.139, 0.178, 0.213	0, 10, 20, 30, 40, 50	0, 0.051, 0.096, 0.139, 0.178, 0.213
SCF	0, 5, 10, 15, 20, 25, 30	0, 0.026, 0.051, 0.075, 0.096, 0.119, 0.139	0, 5, 10, 15, 20, 25, 30	0, 0.026, 0.051, 0.075, 0.096, 0.119, 0.139

The codes employed for the identification of various composites were a combination of alphabets and numerals. For instance, EC is designated to represent a composition of EVA with conductex carbon black filler and so on. NBR and EVA are represented as N and E, respectively; carbon fillers conductex black, printex black, and SCF are designated as C, P, and F, respectively.

Measurement of Electromagnetic Interference Shielding Effectiveness (EMI SE)

The samples were tested for EMI shielding effectiveness by using a Scaler Network Analyzer (HP 8757C, Hewlett Packard) coupled with a sweep oscillator (HP 8350B, Hewlett Packard) within the frequency range 8–12 GHz. The samples for testing used in the experiment were 5.0 mm thick.

RESULTS AND DISCUSSION

EMI shielding effectiveness of the composites

The EMI SE of the composite sets with respect to frequency of radiation (X-band region) are presented in Figure 1. A wave kind of pattern, which is nonlinear and irregular is observed for all sets of NBR and EVA based composites filled with conductex and printex carbon blacks, and carbon fiber. This fluctuation of EMI SE with respect to the frequency of incident radiation can be attributed to the irregular formation of conductive carbon mesh structure in

the polymer matrix and the generation of noise during measurement. It is observed from the Figure 1 (a) and (b) that the increment in EMI SE for conductex black filled composites of both NBR and EVA sets is less than 20 dB over the whole frequency range at its highest filler loading. However, the printex black and SCF filled composites exhibit significantly higher EMI SE compared to the conductex black filled composites at the same level of filler loading. SCF filled composites exhibited the highest of EMI SE compared to other two sets of composites at their same filler loading. For example, if we consider 30 phr loading of fillers, then the EMI SE for conductex black, printex black, and SCF are within 4-7 dB, 35-45 dB, and 45-60 dB, respectively. The reason behind this high EMI SE for printex black and SCF filled composites has been discussed within the next section.

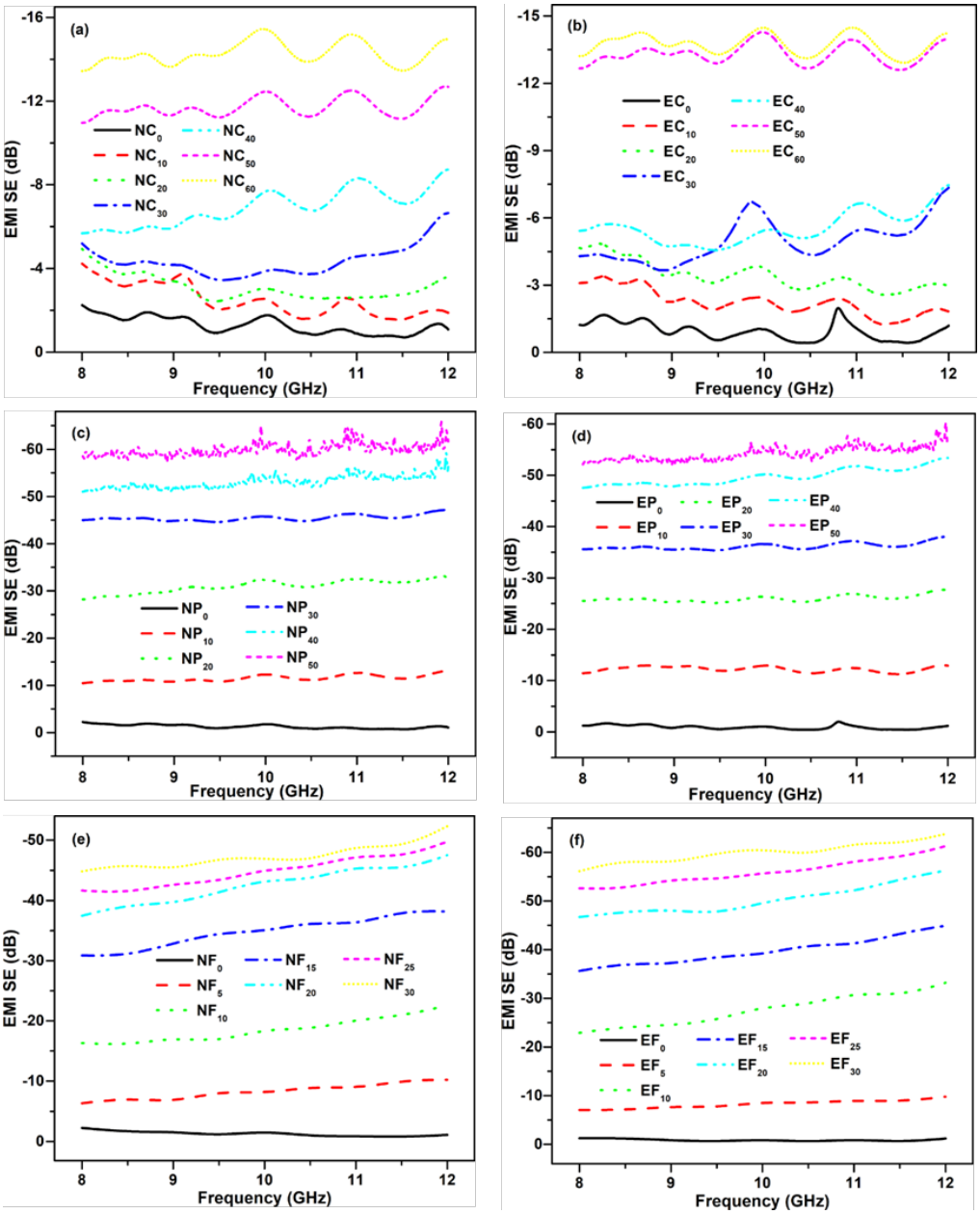

Fig. 1. EMI SE of a) NC, b) EC, c) NP, d) EP, e) NF, and f) EF sets of composites.

Sigmoidal-Boltzmann Model

The use of Sigmoidal Boltzmann model has been reported for use in different areas such as phase transition of smart gels,[32] RF-magnetron co-sputtering in thin films deposition,[33] election of the high-yield subsample within the framework of the compositional nutrient diagnosis system,[34] etc. The Sigmoidal Boltzmann model can be represented as (Eq. 1);

$$Y = A_2 + \frac{A_1 - A_2}{1 + e^{\left(\frac{x - x_0}{\Delta x}\right)}} \quad \text{.....(1)}$$

where Y represents the EMI shielding effectiveness at 'x' volume fraction of filler, which is the corresponding independent variable; A_1 and A_2 are the initial and final values of electrical characteristics, respectively; Δx represents the slope suggesting the gradient of the curve; and x_0 represents the value on the x-axis with respect to the analogous y-axis value denoted by $(A_1+A_2)/2$.

As per the Sigmoidal–Boltzmann model, the PT of EMI SE for NBR and EVA composites with different carbon fillers namely, conductex carbon black, printex carbon black, and SCF have been exhibited in Figure 2b, c, and d, respectively. As explained earlier, the PT is considered as the critical concentration at which there is the first instance formation of a continual conductive network of filler particles within the polymer matrix. This point is also the first instance of a continuous carbon mesh structure formation. This mesh structure is capable of interacting with incident electromagnetic radiation and can potentially absorb it, effectively acting as a shield. Furthermore, the polymer-filler system at the PT changes from insulative to conductive after such filler-filler network formation. Also, loading of filler above the PT leads to the mesh size keeps getting finer, thereby, resulting in closing the gap available for radiation to pass through. As a result, more dense and intense conductive mesh structure is formed with good packing characteristics, which in turn increases the EMI shielding effectiveness value.

Table II gives the values of all other parameters involved to determine EMI shielding effectiveness. It can be observed from Figure 2 and Table II that PTs of NC, EC, NP, EP, NF, and EF based composites are 0.181±0.009, 0.182±0.012, 0.091±0.007, 0.106±0.012, 0.058±0.004, and 0.051±0.007, respectively. It can be observed from the above data that PT are higher for composites with conductex and printex black in comparison with SCF-based NBR and EVA composites. For conductex black, the EMI SE percolation is observed at 0.181 and 0.182 volume fraction, which is almost similar for NBR and EVA matrix composites, respectively. For printex black, the EMI SE percolation is observed at 0.091 and

0.106 volume fraction for NBR and EVA matrix composites, respectively and SCF filled composites exhibit the EMI SE percolation at 0.058 and 0.051 volume fractions for NBR and EVA matrix composites, respectively. Due to the lower viscosity, NBR requires less shearing rate to distribute conductive fillers within its matrix. On the other hand, at the mixing temperature around 45-60 °C, the viscosity of EVA is slightly higher than NBR. Due to higher viscosity, there is comparatively higher shear rate for distributing the conducting fillers within the polymer matrix that results in a larger breakdown of the carbon black structure leading to the splitting of chain-like particles. This phenomenon results in an increase in the PT as more amount of carbon black filler will be required to form the continuous conductive network. However, the PT of NBR based SCF is lower than EVA based composites. The high length and aspect ratio of fibrous carbon (see supplementary section S1) reinforcement within the polymer composite results in a continuous network formation at lower filler loading, thereby, yielding a lower PT.[35] The processing of EVA/NBR composites with particulate black fillers was done in a two-roll mill. On the contrary, the mixing of SCF was carried out in a Haake Rheocord at around 120 °C for 6 min. It is pertinent to note that the temperature of mixing for SCF is almost double to that of roll mill compounding setup. The melting temperature of EVA is reported to be in between 70-80 °C and the system's viscosity further decreases with an increase in mixing temperature. This drop in viscosity as a function of the mixing temperature results in higher fiber length and aspect ratio in EVA composites than NBR composites. The fiber length disintegration in NBR composites is prominent due to its higher viscosity.[35]

The order of percolation limit for various fillers with respect to the volume fraction of filler was observed to be SCF < printex carbon black < conductex carbon black. In the particulate black filled composites i.e., conductex and printex black filled composites, this phenomenon is observed due to a continuous carbon mesh structure formed via aggregates (see supplementary section S1) along with almost equidistant spacing of black particles within the polymer matrix leading to nearly uniform distribution. The ability to have such a mesh structure is rather dependent upon the propensity of the particulate carbon black to form clusters.[36] The carbon particles have a tendency to form primary and secondary carbon structures based on the level of aggregation, which corresponds to the formation of a strong aggregate and the formation of a cluster that has loose packing of primary structured carbon, respectively (see supplementary section S1). A more complex shape and size with a higher presence of internal voids can be termed as a higher carbon structure. The conduction networks are formed more simply within an insulating polymer matrix with a higher

structure. This structural characteristic of carbon black regarding the tendency to form clusters can be predicted from the quantity of dibutyl phthalate absorption by the aggregate. The absorption of conductex and printex carbon black is 115 cc/100 gm and 359 cc/100 gm of carbon black, respectively. Furthermore, the mean particle size and available surface area are 20 nm and 125 m^2/gm for conductex black and 35 nm and 587 m^2/gm for printex black, respectively.[37] Thus, printex black filled composites show a lower PT than conductex black filled NBR and EVA composites.

On the other hand, the SCF with an average length and diameter of 0.12 mm and 6.8 μm[35] is believed to be a linear and large cluster of more than a few carbon blacks (see supplementary section S1), thereby enabling the conductive mesh structure formation. Hence, the EMI SE v/s filler loading percentage curve exhibits the characteristic percolation at the lowermost bulk fraction.[36] The fibrous structure of carbon appears to be very bulky and linear cluster of carbon black particles, which aids the easy formation of a continuous conductive network via an open arrangement of the fiber at much lower loadings in the polymer matrix. Furthermore, the aspect ratio of filler particles plays a very important role in easing the formation of continuous conductive network, as a result of which it reported a lower PT with respect to particulate conductive carbon black filled composites. The network in the case of particulate carbon black had to be built as a result of the aggregation of the filler particles, a role which is played by aspect ratio (length to diameter ratio) in these fibrous fillers. This has to be due to the construction of numerous conductive links that can arrange in a closed mesh type packing within the polymer matrix capable to interrupt with the incident radiation and leads to a more perfect EMI shield formation without leaving any space in the discontinue regions. This structural feature is mostly observed at higher powdered filler percentage within the composite.

The values shown in Table II exhibit different variables achieved by putting in Sigmoidal Boltzmann equation. For an ideal model, the coefficient of correlation (R^2) is equal to 1 with no errors for other variables. The value of R^2 should be 1 for superimposition of curves, which validates the model. The deviation of R^2 value from the unity reflects the errors associated with other variables as shown in Table II. The values of R^2 are close to unity, which show an excellent validation of the SB model for the composite systems under discussion.[31]

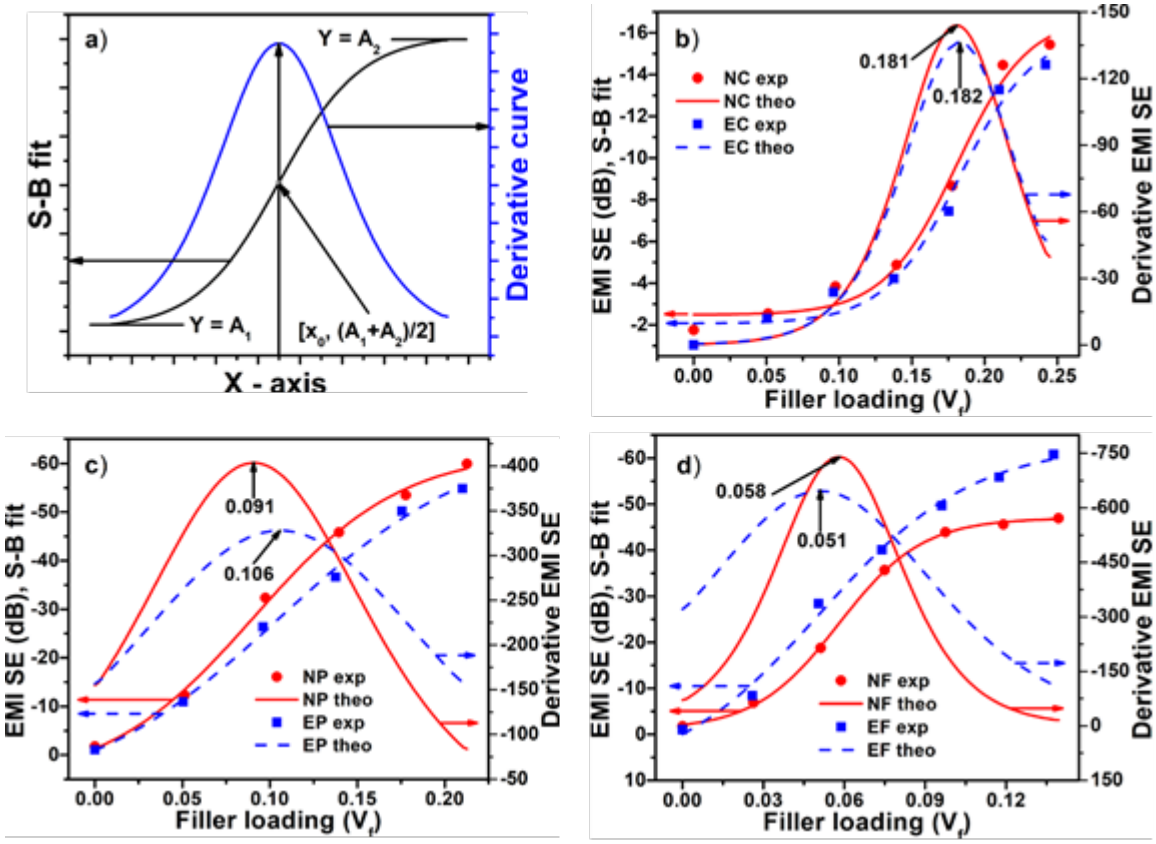

Fig. 2. Experimental, theoretical and derivative graphical curves exhibiting (a) Ideal curve, (b) Conductex black as filler, (c) Printex black as filler and (d) SCF as filler, on the basis of Sigmoidal-Boltzmann model

Table II Parameters based on Sigmoidal-Boltzmann model

SI	A_1	A_2	x_0	Dx	R^2
NC	-02.47±0.59	-16.84±1.72	0.181±0.009	0.025±0.007	0.975
EC	-02.05±0.72	-16.13±2.45	0.182±0.012	0.026±0.010	0.961
NP	05.89±5.16	-62.63±3.38	0.091±0.007	0.042±0.008	0.994
EP	09.29±9.45	-65.79±9.64	0.106±0.012	0.057±0.019	0.991
NF	-00.99±0.68	-47.01±0.44	0.058±0.004	0.016±0.002	0.999
EF	10.43±8.94	-63.14±4.20	0.051±0.007	0.028±0.007	0.989

Sigmoidal–Dose Response Model

The use of Sigmoidal Dose-Response model has been reported for use in various fields such as soil ecotoxicological research,[38] bioassay and radioligand assay for drawing physiological curves,[39,40] study for effect of pyrites sludge pollution on soil enzymes,[41] evaluation of dose response of paclitaxel (anticancer drug) and in microbial risk assessment.[42]

The Sigmoidal Dose response model can be represented with the equation 2 as given below;

$$Y = A_1 + \frac{A_2 - A_1}{1+10^{(\log x_0 - x)P}} \quad \text{.....(2)}$$

where A_1 and A_2 represent the initial (lowest) and final (highest) value of EMI shielding effectiveness, respectively; *log* x_0 represents the midway value between the lowest and the highest value on the Y-axis of EMI shielding effectiveness; *P* represents the slope, suggesting the gradient of the curve around *log* x_0, which is also known as slope factor or hill slope. The slope factor value is unity in the case of a standard dose-response curve. The curve appears to be steeper in case the value of the slope is higher than unity and shallow if it is lower than the same.

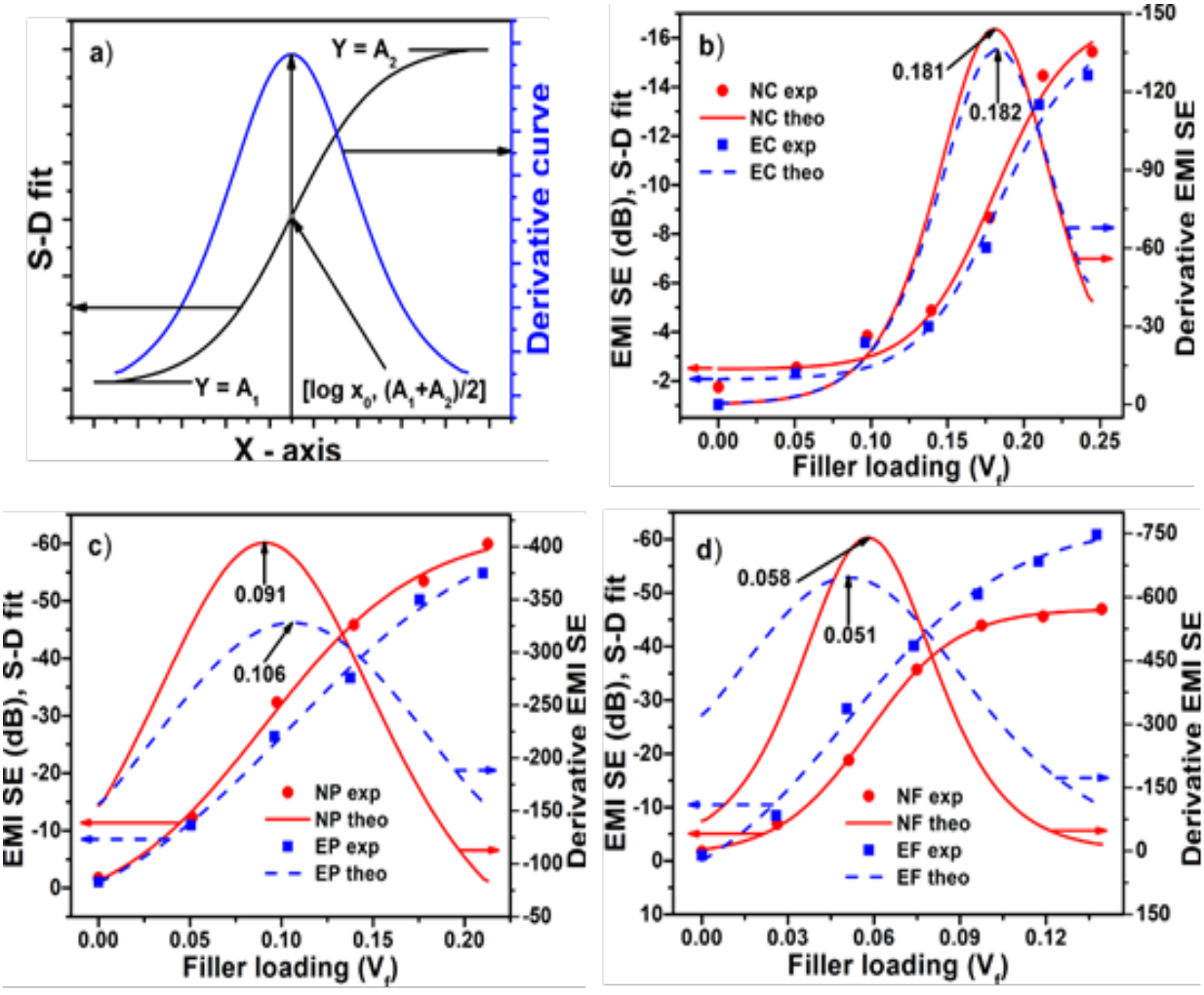

Fig. 3 Experimental, theoretical and derivative graphical curves exhibiting (a) Ideal curve, (b) Conductex black as filler, (c) Printex black as filler and (d) SCF as filler, on the basis of Sigmoidal–Dose Response Model

Table III Parameters based on Sigmoidal Dose Response model.

SI	A_1	A_2	log x_0	P	x_0	R^2
NC	-16.84±1.72	-2.47±0.59	0.181±0.009	-17.43±5.39	1.516	0.975
EC	-16.13±2.45	-2.05±0.73	0.182±0.012	-16.84±6.74	1.523	0.961
NP	-62.63±3.38	5.89±5.16	0.091±0.007	-10.23±2.02	1.232	0.994
EP	-65.79±9.64	9.29±9.45	0.106±0.012	-7.58±2.64	1.275	0.991
NF	-47.01±0.44	-0.99±0.68	0.058±0.002	-27.97±1.50	1.142	0.999
EF	-63.14±4.20	10.43±8.95	0.051±0.007	-15.26±3.95	1.124	0.989

Figure 3(a) represents an ideal graphical curve based on the Sigmoidal Dose-response model as given in equation 2. The PT as shown in Table III along with other variables are determined with the help of derivative curves as shown in Figure 3. Furthermore, in the same equation, $log\ x_0$ gives a measure of the PT. The maximum value of equation 2 given above can be attained with the help of first-order differentiation. Also, the magnitude of maximum value is reached upon by putting second-order differentiation equal to zero $(d^2y/dx^2 = 0)$: as a consequence of which $x = log\ x_0$. The PT, indifferent to SB model is represented here as $log\ x_0$. Figure 3 (b-d) exhibits the PT, which is calculated with the help of derivative curves. Table III gives the values for all other parameters involved to determine EMI shielding effectiveness in the Sigmoidal Response-dose model. The PT determined using the SB model is similar to that of the ones determined using the Sigmoidal Dose-Response model. This can be attributed to the similar value of the *y*-axis parameter for both the models at the PT, which equals to $(A_1 + A_2)/2$. As a result, the alternate method to determine the PT in a graphical way can be by recording the x-axis value, which corresponds to the *y*-axis point as given above i.e. $(A_1 + A_2)/2$. The value of P, the gradient observed at $Y_{50}[(A_1 + A_2)/2]$ implies a sharp increase in EMI SE around the PT for the composite systems as discussed above.

Sigmoidal–Hill Model

The use of Sigmoidal-Hill model has been reported in various fields such as cytotoxic T-lymphocytes and helper cell dynamics in human immunodeficiency virus infection,[43] prediction of emergence of carrot weevil in Canada,[44] adsorption of Chromium (IV) by Codium Tomentosum, a porous media,[45] cellular pharmacodynamics of Duxorubicin,[46] response of weed density to crop yield,[47] etc.

The Sigmoidal Hill model can be represented by the equation 3 as;

$$Y = A_1 + \frac{A_2 - A_1}{1 + \left(\frac{k}{x}\right)^n} \text{.....(3)}$$

Alternatively, it can also be represented by the equation 4:

$$Y = A_1 + (A_2 - A_1)\frac{x^n}{k^n + x^n} \text{.....(4)}$$

Where, *Y* represents the dependent parameter at all volume fractions of '*x*', which is the independent parameter; A_1 and A_2 are initial and final values, respectively of electrical characteristics; *n* represents the hill coefficient, which is also known as hill slope/shape factor and suggesting the gradient of the curve; and *k* represents the filler value on the *x*-axis with respect to the corresponding *y*-axis value denoted by $(A_1+A_2)/2$. The PT is represented by the equation 5 as given below;

$$x = k\left(\frac{n-1}{n+1}\right)^{\frac{1}{n}} \text{.....(5)}$$

which is governed by the hill coefficient magnitude (n>1), and *k*, which is further dependent on A_1 and A_2 values. The PT value *x,* when put in the equation 4 gives us:

$$Y = \frac{A_1 k^n(n+1) + A_2 k(n-1)}{k^n(n+1) + k(n-1)} \text{.....(6)}$$

The above equation represents the corresponding y-axis parameter value at the PT. Figure 4(a) represents an ideal graphical curve based on the Sigmoidal-Hill model. The PT attained from the maxima of graphical curves is shown in Table IV along with other variables as determined with the help of derivative curves shown in Figure 4b -d. The parameters (shown in Table IV), such as A_1, A_2, *k*, *n*, and R^2 are obtained after fitting the experimental data as per equation 4. The PT, that is $k[(n - 1)/(n + 1)]1/n$ was determined with the help of parameters such as *k* and *n* as per equation 5 and shown in Table IV. It can be observed from this table that the PT of NC, EC, NP, EP, NF and EF based composites are 0.178, 0.181, 0.058, 0.085, 0.056, and 0.035, respectively. It is observed that the PT values obtained by fitting of the SH model are lower with respect to the values obtained with the SB model and SD R Model, which holds true for various composite systems as well. Thus, there arises a discrepancy in the results of PT. Actually, the 50% y-axis value (Y50) for the above three models is similar for which the corresponding x-axis values are x_0, $\log x_0$, and *k* for the SB model, SD R model, and SH model, respectively. But, the PT value in case of SH model is not *k* rather it is $k[(n-1)/(n + 1)]^{1/n}$. Since n>1, hence the term $[(n - 1)/(n + 1)]^{1/n}$ is less than unity. As a result, the

PT value determined through SH model show less value compared to the PT values when determined through SB and SDH models. As the value of *n* denotes the gradient of the curve at Y_{50}, it can be observed that there is a steep increase in the EMI shielding effectiveness at Y_{50} and not around the value of the PT as the points are not superimposing and both the values are different.

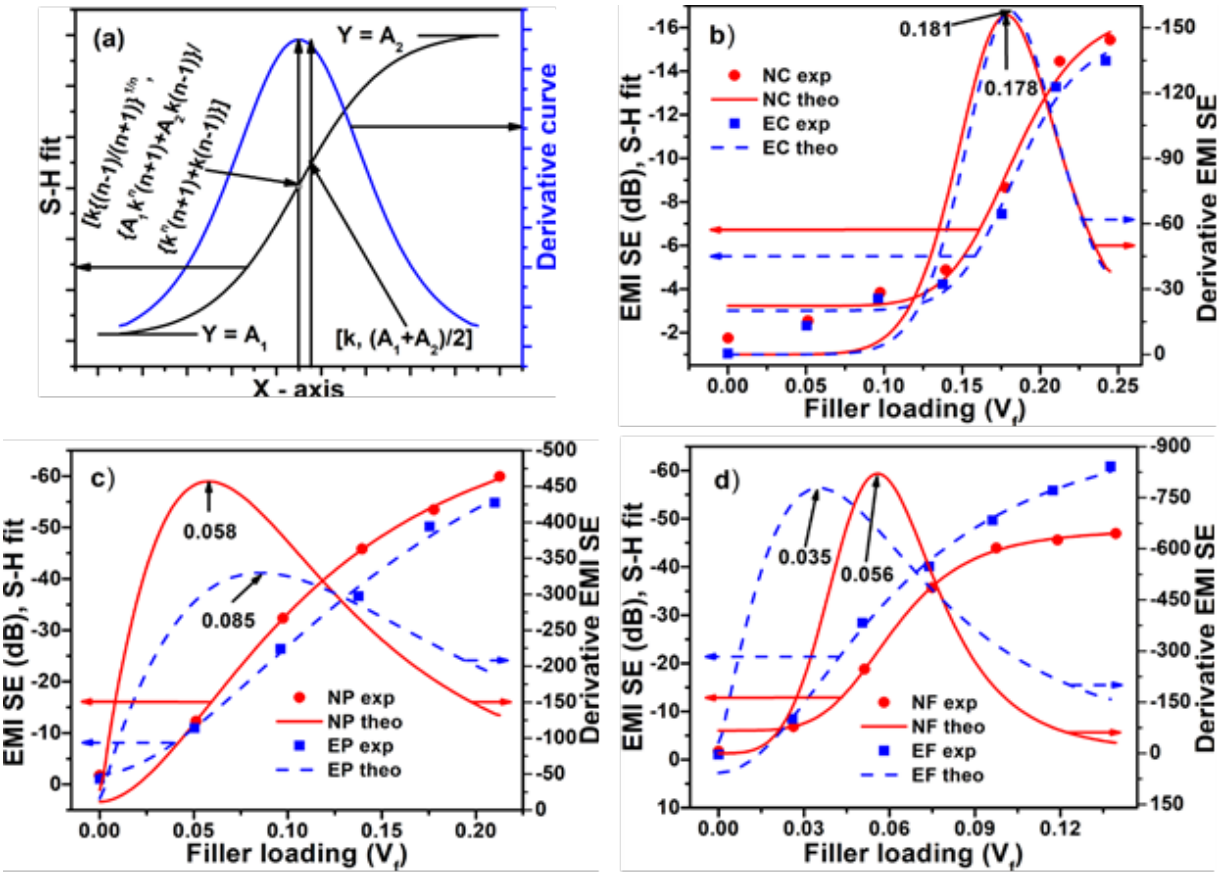

Fig. 4. Experimental, theoretical and derivative graphical curves exhibiting (a) Ideal curve, (b) Conductex black as filler, (c) Printex black as filler and (d) SCF as filler, on the basis of Sigmoidal–Hill Model

Table IV Parameters based on Sigmoidal-Hill model

SI	A_1	A_2	k	n	Xp	R^2
NC	-3.22±0.82	-16.99±2.66	0.1837±0.0125	8.1965±3.9280	0.178	0.961
EC	-3.01±0.93	-15.91±3.21	0.1855±0.0152	8.9564±5.5426	0.181	0.937
NP	-3.40±0.57	-79.63±6.01	0.1138±0.0439	1.8222±3.1387	0.058	0.975
EP	-1.98±0.92	-92.93±8.79	0.1719±0.1466	1.7968±1.7406	0.085	0.990
NF	-6.04±3.07	-47.88±2.75	0.0614±0.0040	4.6003±1.3344	0.056	0.983
EF	-2.73±1.30	-73.13±9.15	0.0627±0.0098	1.9576±1.2277	0.035	0.989

Sigmoidal–Logistic Model

The use of Sigmoidal-Logistic model has been reported for use in various fields such as variability of force during continuous isometric contractions,[48] enzyme inactivation kinetics,[49] growth of plants,[50] phenological model,[51] methane production from thermophilic anerobic digestion,[52] mitigation of biofouling by liquid infused membranes,[53] etc.

This model is consisting of four parameters and can be represented as;

$$Y = A_1 + \frac{A_2 - A_1}{1 + (x/x_0)^P} \quad \text{..... (7)}$$

Where, Y represents the dependent parameter of electrical property at the filler loading x; A_1 and A_2 are the initial and final values, respectively of the electrical characteristics; x_0 represents the midway value of lowest and highest responses, having a similar unit as x, and P represents the gradient of the slope, which is also known as slope factor (>1). The PT is represented as (Eq. 8);

$$x = x_0 \left(\frac{P-1}{P+1}\right)^{\frac{1}{P}} \quad \text{..... (8)}$$

wherein, the value of equivalent point on the y-axis can be represented with the help of equation 9 as given below.

$$Y = \frac{A_1(P-1) + A_2(P+1)}{2P} \quad \text{..... (9)}$$

Figure 5(a) represents the ideal graphical curve based on the Sigmoidal Logistic model as given in equation 7. The experimental and the derivative curves of conductex black, printex black and SCF filled EVA and NBR composites are shown in Figure 5b-d, respectively to determine the PT value. It can be observed that the PT, determined from the maxima of the graphical plots for NC, EC, NP, EP, NF, and EF based composites are 0.176, 0.178, 0.071, 0.083, 0.052, and 0.040, respectively. The values of other parameters like A_1, A_2, x_0, and P are given in Table V for calculating the PT value. The values of x_0 and P were placed in equation 8 for the determination of PT, which has denoted as x_p in Table V. The in-depth investigation of the derivative curves leads us to the general observation that the values obtained by fitting of the S-L model are smaller with respect to the values obtained with the S-B model and S-D R Model, which holds true for various composite systems as well. This discrepancy in the results can be described in the same manner what has been interpreted for SH model. Moreover, the PT values of S-L model are very close to that of S-H model but are dissimilar.

This is because the x-axis point and midway y-axis point in these two models are contrary to each other due to which the equivalent y-axis value is dissimilar at the PT.

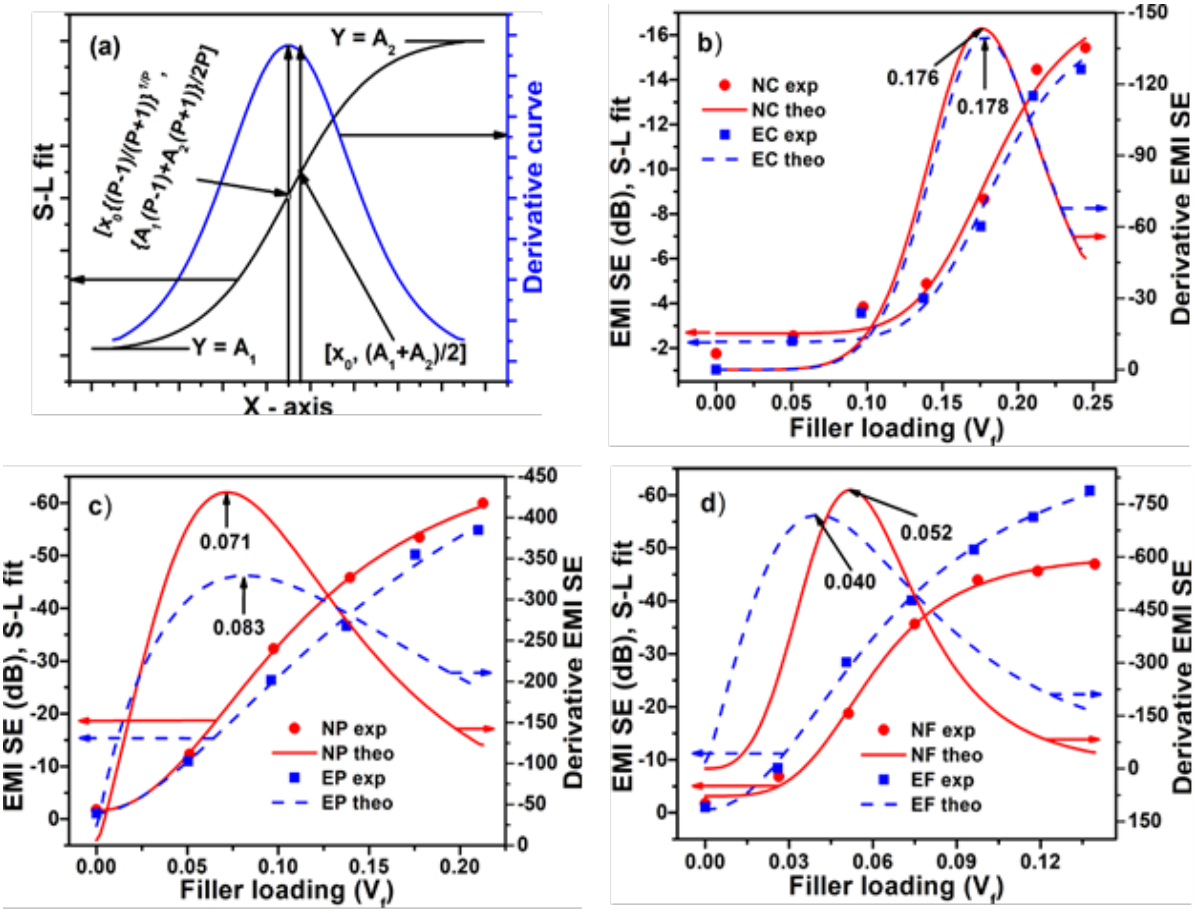

Fig. 5. Experimental, theoretical and derivative graphical curves exhibiting (a) Ideal curve, (b) Conductex black as filler, (c) Printex black as filler and (d) SCF as filler, on the basis of Sigmoidal–Logistic Model

Table V Parameters based on Sigmoidal-Logistic model

SI	A_1	A_2	x_0	P	x_p	R^2
NC	-2.65±0.62	-17.6±2.9	0.183±0.0145	6.86±2.70	0.176	0.967
EC	-2.28±0.71	-16.8±3.8	0.185±0.018	6.99±3.44	0.178	0.951
NP	-1.64±0.74	-74.4±3.7	0.114±0.006	2.16±0.16	0.071	0.998
EP	-1.05±1.99	-97.8±38	0.180±0.084	1.70±0.44	0.083	0.991
NF	-3.14±1.29	-49.1±2.0	0.059±0.003	3.84±0.63	0.052	0.993
EF	-0.60±1.32	-73.6±5.5	0.066±0.006	2.06±0.25	0.040	0.996

Sigmoidal–Logistic-1 Model

The use of Sigmoidal-Logistic-1 model has been reported for use in various fields such as modeling of methane production kinetics,[54] bacterial growth on polyethylene,[55] population growth,[56] cyanide effect on Pseudomonas putida,[57] etc.

This model comprising of three parameters that can be represented by equation 10 as given below;

$$Y = \frac{A_2}{1+ e^{-k\,(x- x_c)}} \quad \text{.....(10)}$$

Where, Y represent the response with respect to electrical properties at the filler loading x; A_2 is the highest electrical property value, k is the gradient of the curve, and x_c is the x-axis value at the sigmoidal half point, which represents the SL-1 model's determined PT. The equivalent y-axis value at the same point is Y=a/2. Figure 6(a) represents the ideal graphical curve based on the SL-1 model; whereas, the derivative curves of EMI shielding for conductex black, printex black, and SCF filled EVA and NBR composites are shown in Figure 6b-d, respectively to determine the PT values. It can be observed that the PT, determined from the maxima of the graphical plots for NC, EC, NP, EP, NF, and EF based composites are 0.233±0.095, 0.236±0.097, 0.096±0.005, 0.111±0.009, 0.057±0.002, and 0.058±0.003, respectively. These values with other parameters are given in Table VI. These calculated PT values through SL-1 model are higher compared to other four models described earlier. This discrepancy in the results may be because of defects within the proposed SL-1 model. During proposition of this model, the experimental value of base material (herein lower limit value) has not been considered and the PT value is calculated based on the upper limit values. Better result could be obtained if the lower limit should be near or equal to zero. However, for the present composite systems, there are lower limit values those are above zero. As a result, the PT values are shifted to the higher values compared to other proposed models. It can also be observed from Figure 6b that the model is not valid for NC and EC composites with conductex black particulate filler within the studied range of filler loading. This is because the gradient of the curve is not sigmoidal over the upper limit region and hence the threshold values are observed on the rightmost top end. It can be said that had there been tests carried out with more filler, the curve would have had more sigmoidal behavior and would have been more fitting and thus valid. The R^2 values are in line with the behavior observed with conductex black filled composites as they are reported to be 0.950 and 0.951 for NC and EC composites, respectively.

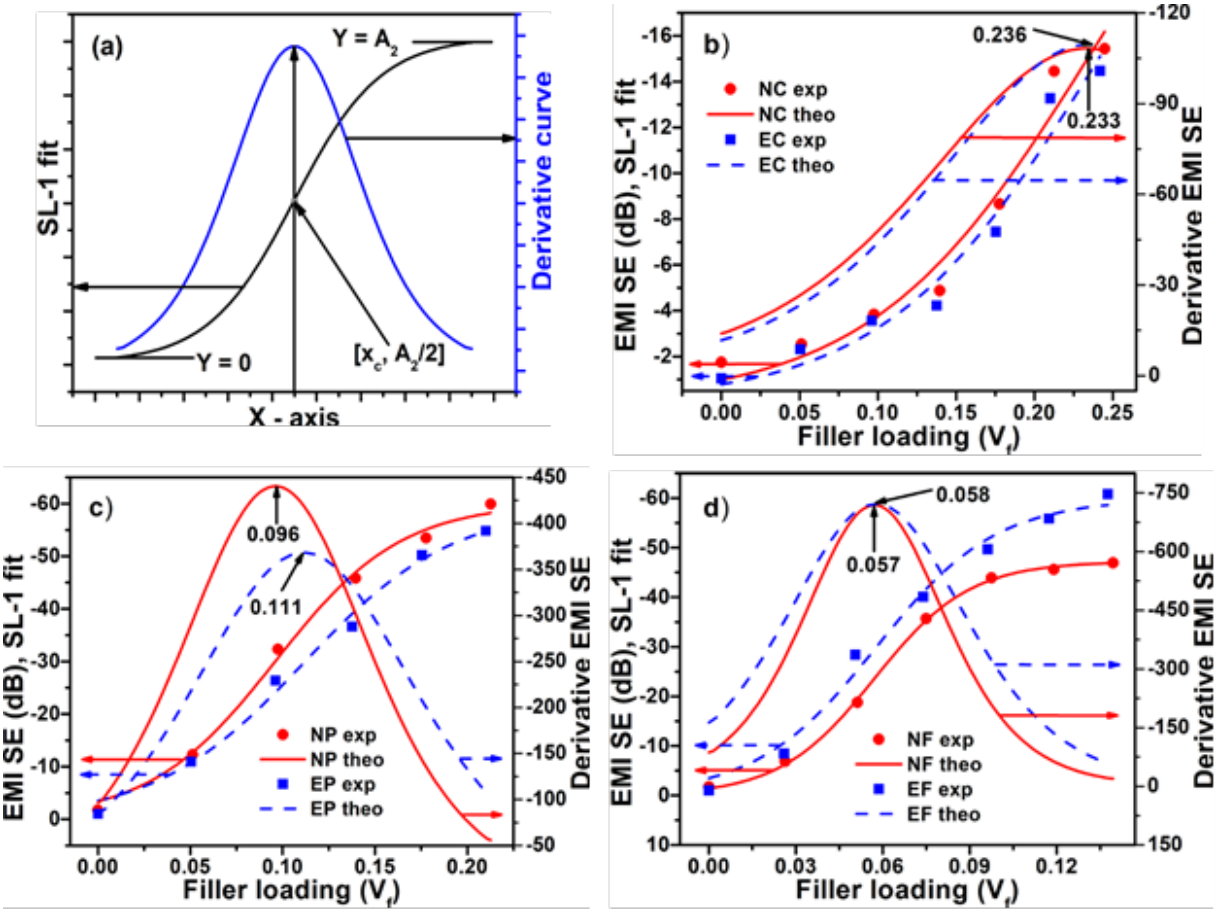

Fig. 6. Experimental, theoretical and derivative graphical curves exhibiting (a) Ideal curve, (b) Conductex black as filler, (c) Printex black as filler and (d) SCF as filler, on the basis of Sigmoidal-Logistic-1 Model

Table VI Parameters based on Sigmoidal-Logistic-1 model

SI	a	x_c	k	R^2
NC	29.88±21.00	0.233±0.095	14.4±5.2	0.950
EC	28.93±22.08	0.236±0.097	15.2±5.6	0.951
NP	60.13±2.43	0.096±0.005	29.3±3.5	0.992
EP	59.44±4.55	0.111±0.009	24.7±4.0	0.987
NF	47.22±0.48	0.057±0.002	60.9±2.5	0.998
EF	59.85±2.91	0.058±0.003	48.2±7.6	0.984

Previously, we have studied and published the percolation threshold of electrical conductivity for the same composite systems determined through these Sigmoidal models.[30] We can compare the percolation threshold result of EMI SE with the percolation threshold of electrical conductivity. It is observed that the percolation thresholds of EMI SE are higher

compared to the percolation thresholds of electrical conductivity when considered all of these Sigmoidal models. Actually, the percolation threshold of electrical conductivity mainly depends on the preferential formation of conductive continuous networks of fillers within the polymer matrix, however, in the case of EMI SE, it depends on the formation of conductive continuous networks as well as the number of mesh size of fillers particles within the polymer matrix. With the progressing addition of fillers, the number of mesh size increases, and hence the percolation threshold is shifted to higher value.

Classical Percolation Theory

The classical percolation theory, the theory of classical particle characteristics intermingling with any random medium for providing an understandable scenario showcasing critical behavior was first proposed in the physics domain by Shante and Kirkpatrick in 1971.[58] It has been recently reported for use in understanding the mechanics of tablet formation via compression and compaction of drug-based powders,[59] connectivity prediction in porous media,[60-61] understand the effects of qubit losses in topological color codes.[62] The equation based on classical percolation theory in the logarithmic form is represented as given in equation 11.

$$log\,\sigma_c = log\,\sigma_0 + t \times \log\left(V_f - V_{fc}\right) \text{.....(11)}$$

Where, σ_c represents the EMI SE value of the composite, V_f represent the volume fraction of fillers, V_{fc} is the volume fraction of filler at PT, t is the critical exponent (1.65-2.0 for three dimensional composite system), and σ_0 is a constant quantity having dimension similar to EMI SE. In this equation $V_f > V_{fc}$. A straight line will be observed if log σ_c is plotted against log $(V_f - V_{fc})$ where the value of t can be obtained from its slope and the value of log σ_0 from its intercept. The plots of log σ_c vs log $(V_f - V_{fc})$ at the best linear fit are shown in Figure 7b and the values of all associated parameters such as PT, critical component, and coefficient of correlation are reported in Table VII. It can be observed from Figure 7a that the EMI shielding effectiveness curves for various polymer composites are similar to that observed via fitting in of the data in various models. The highest shielding effectiveness values are reported for SCF filled polymer composites followed by printex black and conductex black, respectively. The reason for such behavior is already discussed earlier in the paper. Upon comparison of the PT obtained from classical percolation theory with sigmoidal models, it can be seen that the PT obtained by classical percolation theory indicates higher EMI SE

values for EP and NF composites. Furthermore, the EMI SE vs log graph indicates lower gradient and values due to low EMI SE values. The rate of increment for EMI SE depends upon the change in slope with respect to percentage of filler. A higher EMI SE incremental change with filler percentage will generally be resulting in higher slope values. EF has a higher slope than NP in terms of rate of increment.

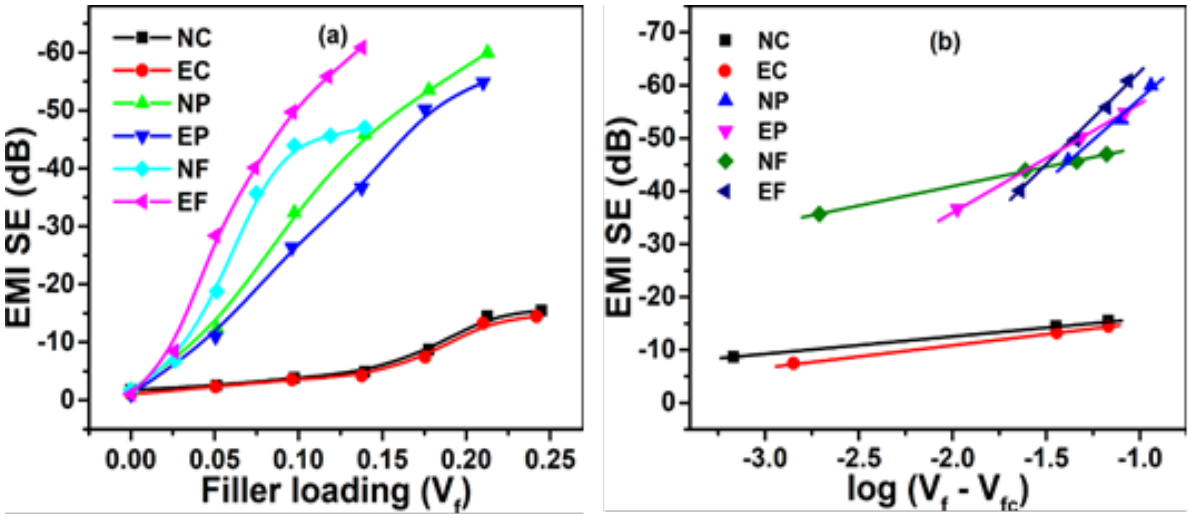

Fig. 7 a) EMI SE of the composite systems with respect to volume fraction of fillers; and b) PT based on classical percolation theory

Table VII Parameters based on classical percolation theory

SN	R^2	Slope	Intercept	PT
NC	0.999	-03.38±0.02	-19.38±0.04	0.177
EC	0.999	-04.18±0.03	-19.33±0.06	0.174
NP	0.974	-31.30±3.58	-88.79±4.14	0.098
EP	0.999	-20.38±0.15	-76.92±0.23	0.127
NF	0.999	-07.34±0.13	-55.60±0.24	0.073
EF	0.995	-35.51±1.48	-98.03±1.96	0.051

From the above going discussion, it is revealed that these models can be applicable to determine the percolation threshold value over certain conditions. To validate SB, SDR, SH, and SL models for the determination of PT value, the nature of experimental curve should be Sigmoidal type. A symmetrical Sigmoidal curve will give the best result of percolation threshold value. As in SL-1 model and classical theory, lower limit (experimental data of base polymer) has not been considered, hence the experimental curve of upper region should be Sigmoidal (asymptotic/exponential) type to be applicable for the determination of

percolation threshold value. To get a symmetrical Sigmoidal curve for any composite system, it is necessary to perfectly select the filler loading gaps and its level. But, in most of the cases, researchers do not follow it.

Other Publications

The potential of various sigmoidal models to determine the PT for reported composite systems is well understood from the discussions done till now. To establish an application relevance of these models for other composite systems as well, an attempt to test these models with EMI SE values in some published literature is done herein.[63-66] The filler loading and EMI shielding effectiveness have been transformed to volume fraction and dB, respectively. The comparative data for EMI SE results as per references[63-66] are for polyethylene waste, PVDF/carbonyl ion composites, composites of ethylene methyl acrylate/ethylene octane copolymer/carbon black composites, and chlorinated PE/carbon black composites, respectively. The results from the above-mentioned work, their sigmoidal fitting curves, and respective derivative curves are presented in Figure 8a-d. The comparative data of PT are tabulated in Table VIII. It can be observed from Figure 8a that the increment rate of EMI SE is less and shifting towards the left-hand side of the plot. Furthermore, 7b indicated that SB and SD models are more valid; whereas, SH and SL models are not valid owing to their non-exponential/non-sigmoidal nature within the studied filler loading range. However, there lies a possibility regarding the validity of these models in case more filler is complemented with more tests done, which would give the curve a chance to be of sigmoidal nature. Figure 8c also represents a sigmoidal nature of the curves for all four models with the highest values of PT among the compared results. Figure 8d is representing the best fitting of the curves with respect to sigmoidal nature. The incremental rate for EMI shielding is less at the initial start, average in the centre, and again less at the end part of the plot. In terms of sigmoidal nature and curve fitting, the hierarchy can be seen as Figure 8d, c, a, and b, from more to less fitting, respectively. SL-1 model is not considered herein with the other publications as it was not valid for any of the selected references.

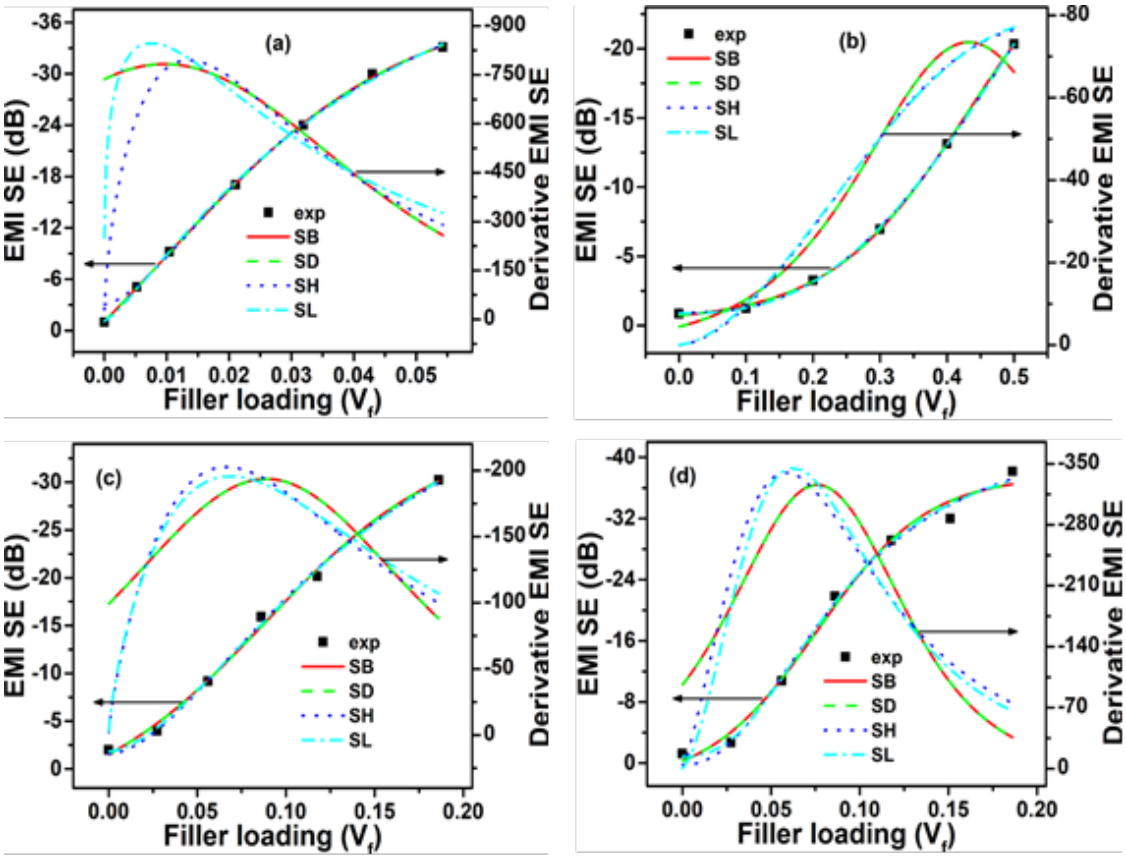

Fig. 8. PT of EMI SE of data taken from (a) Reference[63] (b) Reference[64] (c) Reference[65] and (d) Reference[66] based on different sigmoidal models.

Table VIII EMI PT of some previously published articles based on different Sigmoidal models

SI	PT (Vfc)			
	SB	**SD**	**SH**	**SL**
A[63]	0.001	0.001	0.014	0.008
B[64]	0.432	0.432	-----	-----
C[65]	0.089	0.089	0.067	0.068
D[66]	0.076	0.076	0.058	0.063

PT, determined by the classical percolation theory in this study is lower compared to SL-1 and higher than SB, SD-R, SH, and SL for the majority of composites. It, thereby indicates, that the classical percolation theory calculated PT can be more than, equal, or less than that of the same values based on various sigmoidal models depending upon the EMI SE experimental curve nature. Actually, the calculation of percolation threshold through classical percolation theory is mainly dependent on the nature of experimental curve above the

percolation threshold value that means the upper values of experimental data. This theory is not considering the experimental data of lower values including the base polymer. The experimental curve above the percolation threshold should be exponential in nature. Similar thing happens with SL-1 model where the experimental value of base polymer has not been considered. Hence, the calculation of percolation threshold value based on classical percolation model will be affected if the nature of curve is deviated from its exponential nature. On the contrary, for SB, SD, SH, and SL models, the experimental values of both the base polymer and the highest loaded filler are considered. Hence, herein, the nature of curve over both lower loaded and higher loaded regions are important. For an ideal curve, lower and higher limit/loaded regions should be asymptotic/Sigmoidal in nature and symmetrical on both side of percolation threshold value. But, the experimental curves for polymer composite systems are not like the ideal curve. Mostly, it is non-symmetric, and non-asymptotic on either or both sides. As the nature of curve over both lower and higher loading varies upon composite-to-composite systems, hence it is the exponential nature of curve for classical percolation theory, and asymptotic and symmetrical nature of curves in the case of Sigmoidal models will decide that whether the percolation threshold value determined through classical percolation theory will be higher, equal or less compared to the percolation threshold value determined through Sigmoidal models.

Conclusions

The determination of percolation threshold from different sigmoidal equations has been done on the basis of the highest value for the rate of increase of EMI shielding effectiveness. The PT of EMI SE was determined using different Sigmoidal models such as Boltzmann, Dose-Response, Hill, Logistic, Logistic-1, and classical percolation theory, but SB and SD models indicated similar PT value. This observation is due to the analogous corresponding y-axis values for both these models i.e. $(A_1 + A_2)/2$. The calculated PT values using Hill and Logistic models are dissimilar to each other and are lower with respect to SB and SD models. The results of PT determined by SL-1 model are exhibiting higher values compared to classical percolation theory for only NC and EC composites. The value of R^2, which is close to unity in most of the calculated values is indicative of better curve fitting or physical validity of these Sigmoidal models except for NC and EC composites in the SL-1 model. Although mathematically determined values are influenced by the amount of interval in the data points, the models are easy as only physical fitting is required for their use. These models have also been tested for validation with other composite systems reporting EMI shielding

effectiveness. It is revealed that these models, other than the SL-1 model, can be unanimously employed to determine the PT of EMI shielding effectiveness for filled composite systems though there are some discrepancy within their results. The importance of this study in the field of EMI shielding materials can be in the determination of desirable volume fraction of the filler to be added for polymer composites especially with higher filler loading. It PT of a polymer composite system is known then one can avoid more loading of fillers within the polymer matrix. Thus, this can be proven vital in saving a lot of time and money, which will alternatively be required to do research and development in order to experimentally arrive at the PT.

Acknowledgement

We acknowledge King Saud University, Riyadh, Saudi Arabia, for funding this work through Researchers Supporting Project number (RSP-2021/30).

Conflict of Interest

The authors declare that they have no conflict of interest.

Funding Information

This study was funded by Researchers Supporting Project Number from King Saud University, Riyadh, Saudi Arabia (RSP-2021/30).

References

1. R. J. Chandra, B. Shivamurthy, S. D. Kulkarni, and M. S. Kumar, *Mater. Res. Express* 6, 082008 (2019).
2. T. Williams, in EMC Prod. Des. (Newnes, 1992), pp. 171–210.
3. M.-S. Cao, W.-L. Song, Z.-L. Hou, B. Wen, and J. Yuan, *Carbon* 48, 788 (2010).
4. X. Luo and D. D. L. Chung, *Compos. Part B Eng.* 30, 227 (1999).
5. K. Balasubramanian, M. Tirumali, Y. Badhe, and Y. R. Mahajan, in *Aerosp. Mater. Mater. Technol.* (Springer, 2017), pp. 439–453.
6. Z. Fan, D. Wang, Y. Yuan, Y. Wang, Z. Cheng, Y. Liu, and Z. Xie, *Chem. Eng. J.* 381, 122696 (2020).
7. V. T. Rathod, J. S. Kumar, and A. Jain, *Appl. Nanosci.* 7, 519 (2017).
8. P. Los, A. Lukomska, and R. Jeziorska, *Polimery* 61, (2016).

9. B. Moazzenchi and M. Montazer, *Colloids Surf. Physicochem. Eng. Asp.* 571, 110 (2019).
10. K. Raagulan, J. S. Ghim, R. Braveenth, M. J. Jung, S. B. Lee, K. Y. Chai, B. Mi Kim, and J. Lee, *Nanomaterials* 10, 2086 (2020).
11. L.-C. Jia, D.-X. Yan, Y. Yang, D. Zhou, C.-H. Cui, E. Bianco, J. Lou, R. Vajtai, B. Li, and P. M. Ajayan, *Adv. Mater. Technol.* 2, 1700078 (2017).
12. Y. Xu, Y. Yang, D.-X. Yan, H. Duan, G. Zhao, and Y. Liu, *Chem. Eng. J.* 360, 1427 (2019).
13. J. Han, J. Lee, J. Lee, and J. Yeo, *Adv. Mater.* 30, 1704626 (2018).
14. R. Kumar, A. Sharma, A. Pandey, A. Chaudhary, N. Dwivedi, D. P. Mondal, and A. K. Srivastava, *Sci. Rep.* 10, 1 (2020).
15. A. Sharma, R. Kumar, V. K. Patle, R. Dhawan, A. Abhash, N. Dwivedi, D. P. Mondal, and A. K. Srivastava, *Compos. Commun.* 22, 100433 (2020).
16. J. Varghese, N. Joseph, H. Jantunen, S. K. Behera, H. T. Kim, and M. T. Sebastian, Handb. *Adv. Ceram. Compos. Def. Secur. Aerosp. Energy Appl.* 165 (2020).
17. Z. Liu, G. Bai, Y. Huang, F. Li, Y. Ma, T. Guo, X. He, X. Lin, H. Gao, and Y. Chen, J. *Phys. Chem. C* 111, 13696 (2007).
18. D. D. L. Chung, *Carbon* 39, 279 (2001).
19. S. Sankaran, K. Deshmukh, M. B. Ahamed, and S. K. Pasha, *Compos. Part Appl. Sci. Manuf.* 114, 49 (2018).
20. A. J. Epstein, in *Conduct. Polym. Plast.* (Elsevier, 1999), pp. 1–9.
21. M. H. Al-Saleh and U. Sundararaj, *Carbon* 47, 1738 (2009).
22. J. Liang, Y. Wang, Y. Huang, Y. Ma, Z. Liu, J. Cai, C. Zhang, H. Gao, and Y. Chen, *Carbon* 47, 922 (2009).
23. N. Li, Y. Huang, F. Du, X. He, X. Lin, H. Gao, Y. Ma, F. Li, Y. Chen, and P. C. Eklund, *Nano Lett.* 6, 1141 (2006).
24. Y. Yang, M. C. Gupta, K. L. Dudley, and R. W. Lawrence, *J. Nanosci. Nanotechnol.* 5, 927 (2005).
25. R. Jan, A. Habib, M. A. Akram, I. Ahmad, A. Shah, M. Sadiq, and A. Hussain, *Mater. Res. Express* 4, 035605 (2017).
26. S. H. Lee, S. Yu, F. Shahzad, W. N. Kim, C. Park, S. M. Hong, and C. M. Koo, *Nanoscale* 9, 13432 (2017).
27. S. S. Pradhan, L. Unnikrishnan, S. Mohanty, and S. K. Nayak, *J. Electron. Mater.* 49, 1749 (2020).

28. M. Mishra, A. P. Singh, V. Gupta, A. Chandra, and S. K. Dhawan, *J. Alloys Compd.* 688, 399 (2016).
29. D. Wanasinghe, F. Aslani, G. Ma, and D. Habibi, Nanomaterials 10, 541 (2020).
30. M. Rahaman, A. Aldalbahi, P. Govindasami, N. Khanam, S. Bhandari, P. Feng, and T. Altalhi, Polymers 9, 527 (2017).
31. M. Rahaman, T. K. Chaki, and D. Khastgir, *Adv. Sci. Lett.* 10, 115 (2012).
32. A. L. Navarro-Verdugo, F. M. Goycoolea, G. Romero-Meléndez, I. Higuera-Ciapara, and W. Argüelles-Monal, *Soft Matter* 7, 5847 (2011).
33. J. Reséndiz-Muñoz, M. A. Corona-Rivera, J. L. Fernández-Muñoz, M. Zapata-Torres, A. Márquez-Herrera, and V. M. Ovando-Medina, *Bull. Mater. Sci.* 40, 1043 (2017).
34. E. A. Hernández-Caraballo, O. Rodríguez-Rodríguez, and V. Rodríguez-Pérez, *Environ. Exp. Bot.* 64, 225 (2008).
35. M. Rahaman, T. K. Chaki, and D. Khastgir, *Polym. Compos.* 32, 1790 (2011).
36. N. J. S. Sohi, S. Bhadra, and D. Khastgir, *Carbon* 49, 1349 (2011).
37. M. Rahaman, T. K. Chaki, and D. Khastgir, *J. Mater. Sci.* 46, 3989 (2011).
38. L. Haanstra, P. Doelman, and J. O. Voshaar, *Plant Soil* 84, 293 (1985).
39. A. DeLean, P. J. Munson, and D. Rodbard, Am. J. *Physiol.-Endocrinol. Metab.* 235, E97 (1978).
40. C. Ritz and J. Strebig, *J. Stat. Softw.* 12, (2005).
41. M. B. Hinojosa, J. A. Carreira, J. M. Rodríguez-Maroto, and R. García-Ruíz, *Sci. Total Environ.* 396, 89 (2008).
42. R. L. Buchanan, J. L. Smith, and W. Long, *Int. J. Food Microbiol.* 58, 159 (2000).
43. N. Bairagi and D. Adak, *Chaos Solitons Fractals* 103, 52 (2017).
44. S. Blatt, D. A. Joseph, G. C. Cutler, A. R. Olson, and S. White, *Can. Entomol.* 152, 374 (2020).
45. B. Anandaraj, S. Eswaramoorthi, T. P. Rajesh, J. Aravind, and P. S. Babu, *Int. J. Environ. Sci. Technol.* 15, 2595 (2018).
46. A. W. El-Kareh and T. W. Secomb, *Neoplasia* 7, 705 (2005).
47. S. M. Swinton and C. P. Lyford, *J. Agric. Biol. Environ. Stat.* 97 (1996).
48. E. A. Christou, M. Grossman, and L. G. Carlton, *J. Mot. Behav.* 34, 67 (2002).
49. S. K. Pankaj, N. N. Misra, and P. J. Cullen, Innov. *Food Sci. Emerg. Technol.* 19, 153 (2013).
50. J. Weiner, S. Kinsman, and S. Williams, *Am. J. Bot.* 85, 1638 (1998).

51. S. Kawakita, N. Ishikawa, H. Takahashi, R. Okuno, and T. Takahashi, *J. Agric. Meteorol.* 76, 81 (2020).
52. M. A. Martín, R. Fernández, M. C. Gutiérrez, and J. A. Siles, *Process Saf. Environ. Prot.* 117, 245 (2018).
53. H. Bazyar, L. Xu, H. J. de Vries, S. Porada, and R. Lammertink, *Environ. Sci. Water Res. Technol.* (2020).
54. A. Ware and N. *Power, Renew. Energy* 104, 50 (2017).
55. S. Yahuza, B. I. Dan-Iya, and I. A. Sabo, *J. Biochem. Microbiol. Biotechnol.* 8, 42 (2020).
56. A. Farazmand and M. Amir-Maafi, *Persian J. Acarol.* 7, (2018).
57. M. Abdulrasheed, I. I. Hussein, I. Ahmad, M. M. Namadina, F. Muhammad, and S. Ibrahim, *Bioremediation Sci. Technol. Res.* 8, 27 (2020).
58. V. K. Shante and S. Kirkpatrick, *Adv. Phys.* 20, 325 (1971).
59. S. M. Mishra and B. D. Rohera, *Pharm. Dev. Technol.* 24, 954 (2019).
60. N. Jarvis, M. Larsbo, and J. Koestel, *Geoderma* 287, 71 (2017).
61. B. Tavagh-Mohammadi, M. Masihi, and M. Ganjeh-Ghazvini, *Phys. Stat. Mech. Its Appl.* 460, 304 (2016).
62. D. Amaro, J. Bennett, D. Vodola, and M. Müller, *Phys. Rev. A* 101, 032317 (2020).
63. M. Rahaman, I. A. Al Ghufais, G. Periyasami, and A. Aldalbahi, *Int. J. Polym. Sci.* 2020, (2020).
64. N. Joseph and M. T. Sebastian, Mater. Lett. 90, 64 (2013).
65. R. Ravindren, S. Mondal, P. Bhawal, S. M. N. Ali, and N. C. Das, *Polym. Compos.* 40, 1404 (2019).
66. S. Mondal, S. Ganguly, M. Rahaman, A. Aldalbahi, T. K. Chaki, D. Khastgir, and N. C. Das, *Phys. Chem. Chem. Phys.* 18, 24591 (2016).